

Zero-field NMR study on a spin-glass: Iron-doped 2H—niobium diselenide

M. C. Chen* and C. P. Slichter

Department of Physics and Materials Research Laboratory, University of Illinois at Urbana-Champaign, Urbana, Illinois 61801

(Received 1 April 1982; revised manuscript received 9 August 1982)

We describe a zero-field NMR study attempting to resolve the controversy between phase-transition theories and nonequilibrium glasslike theories of the spin-glass transition. The spin dynamics of Fe spins in 2H-NbSe₂Fe_x is probed through its influence on the nuclear quadrupole resonance (NQR) of ⁹³Nb nuclei. The spin-echo method is used. We measure intensity times temperature, T_{1P} (spin-lattice relaxation parameter), and T_2 (spin-spin relaxation time) as a function of temperature. Our data reveal dramatic differences between non-spin-glass samples ($x=0, 0.25, 1,$ and 5 at. %) and spin-glass samples ($x=8, 10,$ and 12 at. %). Defining the spin-glass transition temperature T_g by the cusp of the susceptibility-versus-temperature curve, we find well-defined minima at $T=T_g$ in intensity times temperature, T_{1P} and T_2 as a function of temperature. Deduction of a correlation time of Fe spins from T_{1P} and T_2 is complicated by the intensity changes which imply that one observes different groups of nuclei at different temperatures. We propose a two-correlation-time model, which utilizes the anisotropy of the exchange interaction, to overcome this difficulty. All of our NQR results and the model calculation of the correlation times of Fe spins are best described by the phase-transition picture of spin-glasses.

I. INTRODUCTION

Spin-glasses have, in recent years, aroused great interest among both theorists and experimentalists. Experimentally, one observes the occurrence of a sharp cusp in the curve of magnetic susceptibility versus temperature at the "spin-glass transition temperature" T_g .¹ In contrast with the antiferromagnetic transition, only a broad maximum of the magnetic specific heat $C_m(T)$ is found at some temperature above T_g .²

Currently there are two opposite theoretical viewpoints attempting to explain this magnetic transition. The main controversy is centered on how a spin-glass state is achieved. The first viewpoint is the phase-transition theory proposed by Edwards and Anderson (EA theory) in 1975.³ In this theory, there is a genuine phase transition at T_g —a sharp change from one thermoequilibrium state (paramagnetic state) to another (spin-glass state). A new kind of order parameter

$$q = \lim_{t \rightarrow \infty} \overline{\langle S_i(t)S_i(0) \rangle}$$

is introduced to calculate the thermodynamic quantities, where the angular brackets mean a spatial average and the overbar a thermal average. The second variety are the nonequilibrium theories, an early version of which is the so-called "cluster model" proposed by Tholence and Tournier (TT model) in 1974.⁴ Such theories view the spin-glass

state as a nonthermoequilibrium state and the spin-glass transition as a kinetic process much in the same way as supercooling a liquid state into a glassy state.

The most natural way to resolve this controversy seems to be the study of the dynamics of magnetic spins. The key physical quantity concerned here is the relaxation rate $1/\tau$ of the spin-autocorrelation function. The phase-transition theory predicts a critical slowing down of $1/\tau$ at T_g similar to that found in magnetically ordered materials.⁵ Several theoretical calculations have been made, but they give different forms and exponents for $1/\tau(T)$.⁶ On the other hand, τ is expected to increase indefinitely with decreasing temperature in the nonequilibrium models.

NMR techniques have been used to study the spin dynamics of spin-glasses. The interpretation of the dynamics of magnetic spins is accomplished through their influence on the host nuclear resonance. In 1977, Levitt and Walstedt found a T_2 minimum of the Cu resonance around T_g in 1 at. % CuMn.⁷ At the same time, MacLaughlin and Alloul observed an intensity minimum of the Cu resonance around T_g in 0.6 and 1 at. % CuMn.⁸ Similar results were obtained in the study of the Al resonance in amorphous manganese aluminosilicates.⁹ Recently, zero-field host NMR signals have been observed¹⁰ below T_g in CuMn and CoGa.¹¹ These results show clearly the appearance of a frozen spin configuration

in the spin-glass state.

The interpretation of host NMR results is complicated by the application of an external magnetic field which is needed in typical NMR experiments. Evidences show that the correlation time might be reduced by the magnetic field.^{12,13} A more important fact is that the susceptibility cusp which is the essential feature of spin-glasses is rounded by a finite magnetic field.¹ Whatever the nature of the spin-glass transition is, it is disturbed by the finite magnetic field. To use NMR to get a clear picture of the spin dynamics of spin-glasses, one must perform the NMR experiments in a zero field.

How can one perform a zero-field NMR experiment to study the spin dynamics of spin glasses? Our approach is to seek a spin-glass system with an observable nuclear quadrupole resonance (NQR), so that no magnetic field is needed to produce a resonance.

Very recently, Coleman and his co-workers found that the iron-doped transition-metal dichalcogenide layer compounds such as $2H\text{-NbSe}_2$, $2H\text{-TaSe}_2$, and $4Hb\text{-TaS}_2$ possess spin-glass-like properties.¹⁴⁻¹⁶ Antoniou¹⁷ developed a model based on the onset of spin-density waves at T_g , instead of a frozen spin configuration, to qualitatively explain these properties. Questions may arise as to whether or not these metallic compounds are "real" spin-glasses like CuMn and AuFe . The essential feature of spin-glasses is generally believed to be the existence of a competition between ferromagnetic and antiferromagnetic exchange interactions. These iron-doped metallic compounds possess this feature and also have a sharp susceptibility cusp. They are anisotropic systems and are sometimes viewed as quasi-two-dimensional systems, while CuMn and AuFe are isotropic systems. However, we believe they are spin-glasses.

These compounds all have a huge electric field gradient. The Nb NMR signal in $2H\text{-NbSe}_2$ has been observed with very good sensitivity.^{18,19} The quadrupole coupling coefficient for Nb in $2H\text{-NbSe}_2$ is found to be $e^2qQ/h = 60$ MHz at room temperature, which makes the largest NQR resonant frequency of Nb ($I = \frac{9}{2}$) about 10 MHz. For the iron-doped $2H\text{-NbSe}_2$, the T_g varies from 4 to 45 K when the atomic concentration of iron changes from 8 to 18 at. %.

Stimulated by the work of Hillenius and Coleman,¹⁶ we have studied both the non-spin-glass samples ($x = 0, 0.25, 1,$ and 5 at. %) and the spin-glass samples (8, 10, and 12 at. %). They very kindly supplied us with the samples on which all of our work was performed. Hillenius and Coleman have reported that $T_g = 4, 7.6,$ and 12 K for the 8, 10, and 12 at. % samples, respectively. We are not the first

group to attempt this kind of NQR study. In 1972, MacLaughlin and Daugherty observed Al NQR in $(\text{La,Gd})\text{Al}_2$.²⁰ The intensity and T_1 were found to decrease with decreasing temperature. Although this is completely different from the results of high-field NMR in the same materials,²¹ no anomaly was found around T_g .

II. INTERACTIONS

In pulsed NMR, the spin echo can only be detected at a finite time τ_d after the rf pulse. Obviously, τ_d must be longer than τ_r , the recovery time of the spectrometer. Then one measures only $M(2\tau_d)$, the magnetization at time $2\tau_d$, instead of $M(0)$. If some nuclei have a T_2 shorter than τ_r , such that $M(2\tau_d)/M(0)$ is much less than 1 for $M(2\tau_d)$ to be measured even after extensive signal averaging, they escape the observation. The NMR signal is also limited by ΔH , the linewidth of the resonance line, in which the inhomogeneous part is usually larger than the homogeneous part. In solids, ΔH is frequently also larger than H_1 (rf field). Then only about $H_1/\Delta H$ of the whole line can be seen. In $2H\text{-NbSe}_2\text{Fe}_x$, there exist several kinds of interactions which a Nb nuclear spin would experience. We shall concentrate only on those interactions which dominate the effects on T_1 , T_2 , and ΔH .

A. Other Nb nuclei

A Nb nuclear spin can interact with other Nb nuclear spins through the dipolar, pseudodipolar, or pseudoexchange interactions. The spin-echo decay caused by these interactions will be described as $M(t)/M(0) = G(t)_{\text{Nb-Nb}}$, which can be a Gaussian, an exponential, or others. The corresponding root second moment $(\langle \Delta\omega^2 \rangle)^{1/2}$, which is independent of temperature, is estimated to be 6×10^3 rad/sec in $2H\text{-NbSe}_2$ single crystal.²²

B. Conduction electrons

The conduction band is a hybridization of d_{zz} with d_{xy} and d_{xx-yy} wave functions. The Nb nuclei are then coupled with the conduction electrons mainly through the core polarization and the spin-orbit interaction¹⁸ which produce a fluctuating local field. The hyperfine field originates mainly from the core polarization and the spin-orbit interaction.¹⁸ This fluctuating local field contributes to both T_1 and T_2 . The T_1 process is characterized by the Korringa relation: $T_1 T = \text{const}$.

C. Fe spins

Doping Fe atoms into $2H\text{-NbSe}_2$ inhomogeneous-

ly broadens the resonance lines both magnetically and electrically. The latter is due to a distribution of electric field gradients (EFG). The more Fe atoms are added, the broader the lines. Magnetically, the Nb nuclear spins interact indirectly with Fe spins via the conduction electrons which are scattered off Fe spins by the d - d exchange interaction. This mechanism provides a motional narrowing effect on the spin-lattice relaxation and the spin-spin relaxation, and is expected to have the opposite temperature behavior to the Korringa process.

Traditionally, this exchange interaction is roughly approximated by the Ruderman-Kittel-Kasuya-Yosida (RKKY) interaction.²³ For the three-dimensional (3D) case:

$$A_0 = (aJ\rho_F/2\pi N)\cos(2k_F R + \phi)/R^3, \quad (1)$$

where A_0 is the hyperfine coupling constant between Nb nuclear spins and Fe spins. This expression is valid only at large R , the distance between Nb spins and Fe spins. In the 2D case which is said to be the limiting case for the layer compounds, A_0 contains $\sin(2k_F R + \phi)/R^2$ instead. In Eq. (1), $a = \gamma\hbar H_{\text{hf}}$ is the hyperfine coupling constant between nuclear spins and the conduction electrons, J is the strength of the d - d exchange interaction, ρ_F is the electron single spin density of states at the Fermi level, N is the density of the conduction electrons, and k_F is the wave vector at the Fermi level. These parameters can be estimated from NMR, Hall coefficients, specific heat, and superconductivity transition-temperature measurements, and from the free-electron model, respectively. So, the exchange field produced by Fe spins at Nb spin sites can then be estimated.

Generally, the exchange field produced by Fe spins at Nb nucleus i can be written in the following general form:

$$h(t)_{ip} = \sum_{kp'} A_{ik,pp'} \mu(t)_{kp'}. \quad (2)$$

In this equation, the subscript p is used to denote coordinate components x , y , and z . Thus, $\mu(t)_{kp'}$

means the p' component of the magnetic moment from Fe spin k . It can be decomposed into a static part $\overline{\mu(t)_{kp}}$ and a dynamic part $[\mu(t)_{kp} - \overline{\mu(t)_{kp}}]$, where the bar means, again, a time average. $\mu(t)_{kp}$ can contribute to ΔH and is nonzero in an external magnetic field. It is proportional to the magnetic field with the spin susceptibility χ_p as the proportional coefficient. In this case, a static exchange field h_{ip} is produced at the Nb nucleus i . In spin-glasses and in a zero field, both the EA phase-transition theory and the nonequilibrium model predict $\overline{\mu(t)_{kp}} = 0$ above T_g and $\overline{\mu(t)_{kp}} \neq 0$ below T_g , where a frozen spin configuration exists. We thus expect no temperature dependence of ΔH from the exchange interaction with Fe spins above T_g .

III. REDFIELD THEORY OF RELAXATION TIMES

The concept of a nuclear spin temperature is not usually valid in pure NQR because the unequally spaced energy levels inhibit the mutual spin flips necessary to establish a spin temperature.²⁴ Then one does not expect an exponential spin-lattice relaxation process. We must use the density matrix technique to calculate the equations of motion for both the spin-lattice relaxation process and the spin-spin relaxation process. Redfield theory provides a general set of linear differential equations for the elements $\rho_{mm'}$ of the density matrix.²⁴ This set of equations is valid only when T_1 and T_2 are much longer than τ , the correlation time of perturbations. This is exactly the condition of the validity of the motional narrowing limit.

In $2H\text{-NbSe}_2$, Nb nuclei have spin $\frac{9}{2}$, there are five energy levels with a twofold Kramers's degeneracy between $I_z = \pm m$ states. If we write $e^2 q Q / 24 \hbar = \omega_0 = 2.5$ MHz and carry out the calculation for the off-diagonal parts: $\rho_{9/2,7/2}$, $\rho_{7/2,5/2}$, etc., we get T_2 decay forms for these transitions. The result is a single exponential. For the $\frac{9}{2} - \frac{7}{2}$ transition (resonant frequency = $4\omega_0$),

$$1/T_2 = (\gamma^2/4) \{ 2k_{zz}(0) + 18[k_{xx}(4\omega_0) + k_{yy}(4\omega_0)] + 16[k_{xx}(3\omega_0) + k_{yy}(3\omega_0)] \}, \quad (3)$$

where k_{pp} is the p component of the real parts of the spectral densities of the fluctuating local fields. And

$$k_{pp}(\omega) = h_p^2 \tau / (1 + \omega^2 \tau^2)$$

is obtained if a simple exponential autocorrelation function is assumed, where h_p^2 is the p component of the square amplitude of the fluctuating local field. One important result is that T_2 is "transition dependent." The higher transitions have larger T_2 than the lower transitions.

k_{pp} is actually the Fourier transform of the autocorrelation function of the fluctuating local fields, $F(\tau)_{pp}$. This autocorrelation function of Nb nucleus i is defined as

$$F(\tau)_{ipp} = \overline{h(t)_{ip} h(t+\tau)_{ip}}.$$

From Eq. (2), it can be easily shown that

$$F(\tau)_{pp} = \{F(\tau)_{ipp}\}_i = \sum_{kp'} \{A_{ik,pp'}^2\}_i [\overline{\mu(t)_{kp'}\mu(t+\tau)_{kp'}} - \overline{\mu(t)_{kp'}}\overline{\mu(t+\tau)_{kp'}}], \quad (4)$$

where the curly brackets mean an average over all Nb nuclei. During the derivation of Eq. (4), we have used the fact that the cross terms between different Fe spins k are averaged to zero when an average over all Nb nuclei i is done, i.e., $\{A_{ik,pp'}A_{ik',pp'}\}_i = 0$. This is because the interaction from Fe spins is an oscillatory function of distance between Fe spins and Nb nuclear spins. One assumption has also been made that the fluctuations of the three components of magnetic moments are independent. This makes cross terms like $\overline{\mu(t)_{kp'}\mu(t+\tau)_{kp'}}$ equal to zero.

From the definition of the EA order parameter q , we see that the second term of Eq. (4) is closely related to q . But here, each spatial component is weighted differently because of the possibility of the directional dependence of $\{A_{ik,pp'}^2\}_i$. However, we expect the mean-square amplitude of the fluctuating local fields to be temperature independent above T_g , and to decrease approximately as $(1-q)$ below T_g .

For the T_1 process, we calculate the diagonal parts: $\rho_{9/2,9/2}$, $\rho_{7/2,7/2}$, etc. We have a set of five coupled linear differential equations, where the adjacent levels are coupled among one another. We get the following form for the relaxation matrix A as defined in Ref. 25, where a "master equation" approach is used to get the decay forms of the population difference:

$$A = \begin{vmatrix} 18a & -16b & 0 & 0 \\ -9a & 32b & -21c & 0 \\ 0 & -16b & 42c & -24d \\ 0 & 0 & -21c & 48d \end{vmatrix},$$

where $a = \gamma^2[k_{xx}(4\omega_0) + k_{yy}(4\omega_0)]/4$. Similar expressions for b , c , and d are obtained by substituting $4\omega_0$ with frequencies $3\omega_0$, $2\omega_0$, or ω_0 .

If we assume $\omega_0\tau \ll 1$, we have $a = b = c = d$ and

$$1/T_{1P} = 2a = (\gamma^2/2)(k_{xx} + k_{yy}). \quad (5a)$$

By further assuming the isotropy of the correlation times (μ_x , μ_y , and μ_z have the same correlation time τ), $k_{pp}(\omega)$ becomes $h_p^2\tau$, and

$$1/T_{1P} = \gamma^2(h_x^2 + h_y^2)\tau/2. \quad (5b)$$

This definition of T_{1P} can be related to the spin-lattice relaxation time, T_{1H} , which would be obtained in high-field NMR. For the case in which there is a static magnetic field and no quadrupole splittings, the spin-lattice relaxation has a single ex-

ponential decay. If one has the same fluctuating local fields as in Eq. (5b), T_{1P} would be equal to T_{1H} . We shall call T_{1P} the "spin-lattice relaxation parameter." From relaxation matrix A , we get a multiexponential decay for the T_1 process. Different transitions have a common T_{1P} , but the coefficients for each "normal-mode" exponential are different.²⁵

The same conditions used in Eqs. (5a) and (5b) also change Eq. (3) into

$$1/T_2 = \gamma^2/2[k_{zz} + 17(k_{xx} + k_{yy})] \quad (6a)$$

and

$$1/T_2 = \gamma^2[h_z^2 + 17(h_x^2 + h_y^2)]\tau/2. \quad (6b)$$

Then assuming that the fluctuating local field is isotropic ($h_x^2 = h_y^2 = h_z^2$), we have, for the $\frac{9}{2} - \frac{7}{2}$ transition only, $T_{1P}/T_2 = 17.5$. The measurement of this ratio can provide a test of whether or not the isotropy of the correlation times applies.

The observed T_{1P} of Nb nuclei should be written as

$$(1/T_{1P})_{\text{obs}} = (1/T_{1P})_{\text{CE}} + (1/T_{1P})_{\text{Fe}}, \quad (7)$$

where the subscript CE means the contribution from the conduction electrons. In the future treatment of T_{1P} data, the Fe spin's contribution can be pulled out simply by subtracting $(1/T_{1P})_{\text{CE}}$, as will be deduced from the pure sample, out of the observed T_{1P} rate.

For the T_2 relaxation, besides the above two T_1 mechanisms, there is the spin-spin interaction between Nb spins. This interaction is a slow process. Redfield theory cannot be applied to it. One writes

$$M(t)/M_0 = \exp[-t/(T_2)_{\text{CE}}] \times \exp[-t/(T_2)_{\text{Fe}}]G(t)_{\text{Nb-Nb}} \quad (8)$$

for the decay of the spin-echo amplitude. The correction can then be made by moving terms (it depends on what correction shall be made) from the right-hand side of Eq. (8) to the left-hand side (this will be the experimental data) on the computer.

In the motional narrowing limit and for isotropic correlation times, Eqs. (5b) and (6b) also become

$$(1/T_{1P})_{\text{Fe}} \text{ or } (1/T_2)_{\text{Fe}} = \gamma^2 h_L^2 \tau, \quad (9)$$

where h_L is the fluctuating local field, which depends on how far a Nb spin is from a Fe spin. Its value can be roughly estimated with Eq. (1) as explained earlier. It is then obvious that the study of

T_{1P} and T_2 of Nb spins would provide us with some information about τ , the correlation time of Fe spins.

IV. EXPERIMENTAL

A. Samples

All the $2H\text{-NbSe}_2\text{Fe}_x$ powder samples, except the pure sample, used in this experiment were kindly loaned to us by Professor R. V. Coleman of the University of Virginia (Charlottesville). The pure sample was prepared by the same procedures as Hillenius and Coleman used to prepare their samples for the susceptibility measurements.¹⁶ The resulting powder was sieved with a No. 200 mesh to keep particles with sizes smaller than $75\ \mu\text{m}$. We checked the crystalline structure of this pure sample and the borrowed 0.25-at. % sample with x-ray diffraction. They have exactly the same x-ray powder patterns. The positions of peaks are also consistent with those reported in the literature for $2H\text{-NbSe}_2$.²⁶

B. Spectrometer

We followed an add-subtract technique to measure T_1 and T_2 by spin echoes. This technique was based on a method of D. M. Follstaedt and D. C. Barham,²⁷ modified by our group. The T_2 sequence is $\pi/2 - \tau_d - \pi$ (0° phase, add) $(-\pi/2) - \tau_d - \pi$ (180° phase, subtract). The T_1 sequence is $\pi/2 - \tau_w - \pi/2 - \tau_d - \pi$ (add) $\pi/2 - t_w - (-\pi/2) - \tau_d - \pi$ (subtract). In the T_2 sequence, τ_d is varied to map out the spin-echo decay curve, while τ_w is changed in the T_1 sequence. This method eliminates the coherent noise which follows the rf pulses, thus allows the use of a τ_d as short as possible. The advantage of using our version of the T_1 sequence is that the base line [$M(\infty)$] of the T_1 decay curve is subtracted out during the measuring process. This allows us to measure points at the tail more accurately than the conventional $\pi/2 - \tau_w - \pi/2 - \tau_d - \pi$ sequence.

All the samples were mixed with fine Al_2O_3 powder to reduce eddy-current effects. They were encapsulated in nylon containers. Small holes were drilled on the container's cap, which was then covered with filter paper and sealed with epoxy. This allows liquid helium to flow into the container to ensure good cooling at low temperatures.

An external tuning technique was adopted due to the temperature dependence of the coil's Q value, which caused the tuning to drift with temperature. The tuning capacitors were placed inside a brass box external to the dewar. This scheme makes good tuning possible at any temperatures. We suffered from

acoustic ringing effects at low temperatures even in a zero magnetic field. It was sample dependent, and occurred only when the T_g of each sample was approached. A coil wound with stranded wire was used to cut down this ringing to a tolerable extent. The H_1 (rf field) used through this experiment is estimated to be about 100 G at 200 W.

A Janis Super Varitemp Dewar was used to vary the temperature from 300 to 1.6 K. A calibrated 1/8-W, 560- Ω Allen Bradley carbon resistor was used to read the temperature above 4.2 K. The resistance of the thermometer at 77 and 4.2 K has been constantly checked since the calibration. The drift was found to be about 3% in terms of $\delta T/T$ after one year's extensive use. For temperatures between 4.2 and 1.6 K, we pumped the dewar with the probe can immersed in liquid helium. The temperature was measured by reading the vapor pressure on a Wallace and Tiernan gauge (0–100 mm Hg).

C. Susceptibility rig

An ac mutual inductance bridge was constructed. This bridge is easy to build and needs only a small ac magnetic field (several gauss) to get 10^{-7} emu/g sensitivity. It is ideal for the detection of the susceptibility cusp in spin-glasses around the T_g . Two secondaries with 1000 turns of No. 34 copper wire were wound on two separate sections of a machined nylon form. The primary had 2500 turns of No. 34 copper wire and was wound on top of two secondaries with a layer of thin Mylar sheet between them. The GE 7031 varnish-toluene mixture was painted on the coil every two or three layers during the winding.²⁸ Two secondaries were connected in the opposite direction so that their induced voltage can be compared. We followed the bridge circuit designed by C. M. Brodbeck *et al.*²⁹ to provide an electronic version of the variable mutual inductor, but with some modifications. The bridge was driven and detected by a PAR HR-8 lock-in amplifier at 500 Hz. The ac magnetic field produced by the primary is estimated to be about 0.5 G.

V. RESULTS AND DISCUSSIONS

We used two different ways to measure the intensity for two different studies. In the line-shape study (to measure the linewidth), the intensity was measured at a fixed time (τ_d) as the integrated spin echo. In the intensity study as a function of temperature, it was measured as the spin-echo amplitude extrapolated to time zero. In other words, it was obtained as a result of the T_2 measurements. And it was measured at 10.15 MHz for all the samples. An H_1 of 100 G was used and kept constant

through the entire measuring temperature range (300–1 K). From the resistivity measurements,³⁰ the dilute non-spin-glass samples can be estimated to have a skin depth which varies from 160 to 70 μm over the whole temperature range. For the spin-glass samples, the skin depth was about 160 μm and has very little temperature dependence. We therefore conclude that the temperature dependence of the skin depth will not cause a large deviation in the intensity from Curie's law.

A. Linewidth measurements

The linewidth is defined as the full width at half maximum (FWHM). One can use the frequency dependence of the linewidth to determine whether the mechanism of the inhomogeneous broadening is of electric or magnetic origin. If it is due to the magnetic effects, the linewidth should be independent of which transition is involved (e.g., $\frac{9}{2}-\frac{7}{2}$ or $\frac{7}{2}-\frac{5}{2}$). The linewidth would be proportional to the resonant frequency of the transition, if it is due to a random distribution of static electric field gradients (EFG). At 77 K, the $\frac{9}{2}-\frac{7}{2}$ transition and the $\frac{7}{2}-\frac{5}{2}$ transition have the same linewidth in all samples, and the linewidth increases proportionally to the concentration up to 5%; then it saturates at higher concentrations.

At 23.1 K, the resonance line of each transition splits into two peaks in the pure and 0.25-at. % samples. The separation between these two peaks is proportional to the peak resonant frequency. This is a proof that the splitting is caused by the EFG's induced by charge-density waves (CDW) ($T_c = 36$ K in the pure sample). These two peaks collapse into a central peak again in the 1-at. % sample [Fig. 1(a)]. This is consistent with the Hall-coefficient measurements³¹ that the CDW transition is completely quenched by doping 0.6 at. % of Fe in $2H\text{-NbSe}_2$. The linewidth is proportional to the resonant frequency, showing it is of electric quadrupole origin. This observation together with the line-shape study and the Hall-coefficient measurements show that the CDW only loses the long-range order in the 1-at. % sample, but it still exists in the short range.

The linewidth is the same for the two transitions ($\frac{9}{2}-\frac{7}{2}$ and $\frac{7}{2}-\frac{5}{2}$) in the higher-concentration samples (5 at. % and up) at 23.1 K, as shown in Fig. 1(b), indicating that magnetic effects are more prominent here than the CDW effects even at low temperatures. For the same sample, the linewidth changes very little when the temperatures changes from 77 to 23.1 K. In contrast, it increases several times in the 1-at. % and more dilute samples over the same temperature range.

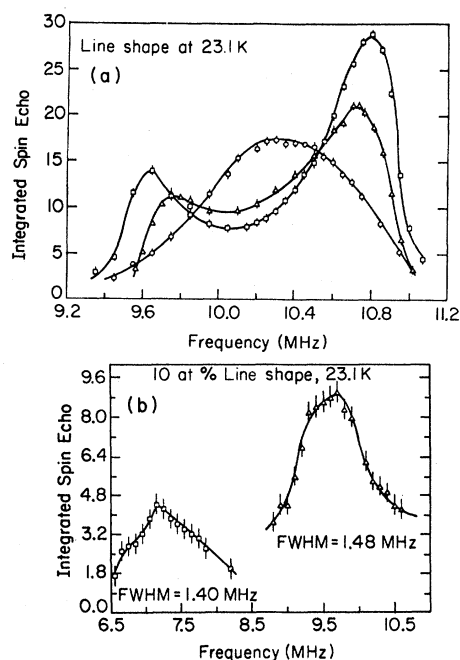


FIG. 1. (a) Line shapes for the pure, 0.25-, and 1-at. % samples at 23.1 K. The solid line is a guide for the eyes. \square : pure, \triangle : 0.25, \circ : 1 at. %. (b) Line shapes for the $\frac{9}{2}-\frac{7}{2}$ (peak frequency = 9.7 MHz) and $\frac{7}{2}-\frac{5}{2}$ (peak frequency = 7.15 MHz) transitions for the 10-at. % sample at 23.1 K. The ratio of peak frequencies for these two transitions is about 0.74, very close to the theoretical value of $\frac{3}{4}$.

B. T_2 at 10.15 MHz

The spin-echo decay curves of the non-spin-glass samples are neither Gaussians nor exponentials. At short times they are exponentials, but become Gaussians at longer times. Later analysis will explain the mechanisms behind this kind of decay. As the temperature is lowered, it takes longer and longer time to decay down to $1/e$ of $M(0)$ in the pure, 0.25- and 1-at. % samples. This $1/e$ decay time does not change with temperature in the 5-at. % sample. For all spin-glass samples, the decay curve is a single exponential throughout the entire measuring temperature range, and T_2 decreases with decreasing temperature to develop a shallow minimum around T_g (Fig. 2). The change of T_2 is only about a factor of 3 over the entire measuring temperature range. At 77 K and 10.15 MHz, T_2 decreases slightly with increasing concentration in the spin-glass samples.

C. T_{1P} at 10.15 MHz

T_{1P} is obtained by finding the best fit of the experimental data to the calculated T_1 decay curves.²⁵ We have studied the T_1 decay curves at the peak

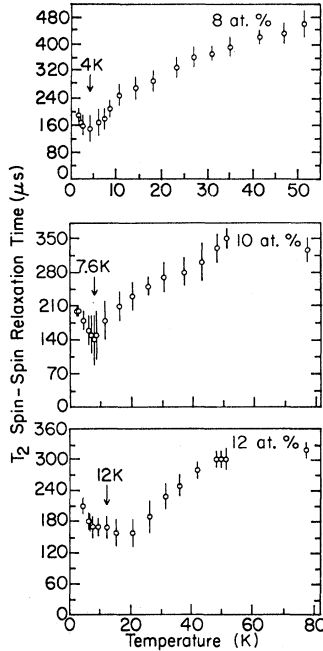


FIG. 2. T_2 as a function of temperature for three spin-glass samples.

resonant frequencies of $\frac{9}{2}-\frac{7}{2}$ and $\frac{7}{2}-\frac{5}{2}$ transitions in the 1, 5, and 10 at. % samples at 77 and 4.2 K. It is found that one can use a single parameter T_{1P} to fit these two decay curves fairly well.

At 77 K, T_{1P} does not change among the pure, 0.25 and 1 at. % samples. It then decreases slightly with increasing concentration, as T_2 does. $T_{1P}(T)$ obeys a $1/T$ behavior (Korringa relation) fairly well in the pure sample and not as well in the 0.25 at. % sample. We get $T_{1P}T \sim 900$ ms in the pure sample and $T_{1P}T \sim 700$ ms in the 0.25 at. % sample. These values are a bit higher than the 500 ms reported in the literature.^{18,32}

In the 5 at. % sample, after a broad T_{1P} maximum at about 17 K, T_{1P} decreases with decreasing temperature (Fig. 3). But in the 10% sample, T_{1P} has not only a broad maximum at about 37 K but also a shallow minimum around T_g ($=7.6$ K), where a T_2 minimum has already been observed. Again the overall change of T_{1P} is only about a factor of 2 or 3 over the entire measuring temperature range. The T_{1P} maximum can readily be understood as the result of the interplay between the contributions from the conduction electrons and from Fe spins.

D. Treatment of T_1 and T_2 data

From the temperature dependence of $1/e$ decay time of the T_2 decay in the pure, 0.25 and 1 at. % samples, we shall assume the interaction with Fe

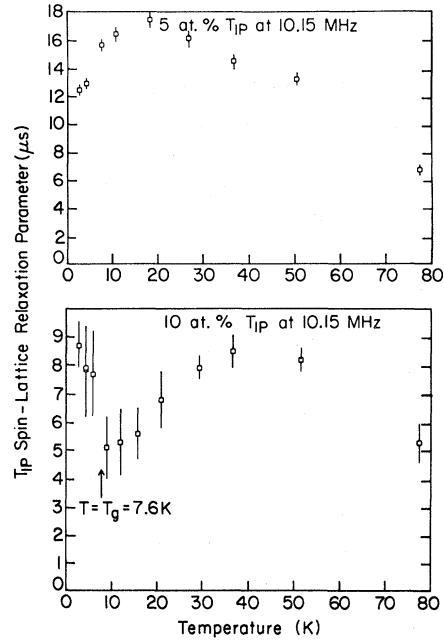


FIG. 3. T_{1P} as a function of temperature for the 5 at. % (non-spin-glass) and 10 at. % (spin-glass) samples.

spins is not important in these samples. Equation (8) (for the spin-echo decay) can be rewritten as

$$M(t)/M_0 = \exp[-17.5t/(T_{1P})_{CE}G(t)_{\text{Nb-Nb}}], \quad (10)$$

where the contribution from the conduction electrons is represented by $17.5/T_{1P}$ as predicted by Redfield theory. $(T_{1P})_{CE} = 900$ ms/T has been chosen as the standard T_{1P} from the conduction electrons. Equation (10) is then used to pull out $G(t)_{\text{Nb-Nb}}$ from the T_2 decay curves at each temperature. $G(t)_{\text{Nb-Nb}}$ is found to be a Gaussian function. If we define a Gaussian decay as $M(t)/M_0 = \exp(-t^2/T_2^{*2})$, then the corresponding linewidth is $2(\ln 2)^{1/2} (2/T_2^*)$. We assign $T_2 = T_2^*/2(\ln 2)^{1/2}$ as our Gaussian T_2 , so the corresponding homogeneous linewidth is simply $2/T_2$.

Figure 4 shows the residual Gaussian T_2 , $(T_2)_{\text{Nb-Nb}}$, after the subtraction. This $(T_2)_{\text{Nb-Nb}}$ not only has very little temperature dependence but also has closely similar values in three dilute samples. This is a qualitative proof that the residual interaction is indeed the Nb-Nb dipolar interaction. These samples have an average $(T_2)_{\text{Nb-Nb}}$ of about 1100 μs . This corresponds to a dipolar halfwidth (or $\langle \Delta\omega^2 \rangle^{1/2}$) of 3×10^3 rad/s, very close to the value reported in the literature (Sec. II A). We thus have a quantitative basis to justify this data-processing procedure. For the 5 at. % sample, the influence from Fe spins becomes important, $17.5/(T_{1P})_{\text{obs}}$ is used in

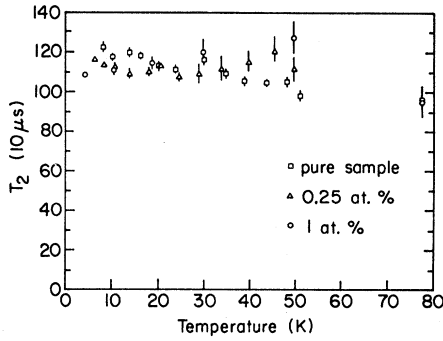


FIG. 4. Gaussian T_2 of the Nb-Nb dipolar interaction as a function of temperature for the pure, 0.25-, and 1-at. % samples.

Eq. (10) to represent the contributions from two T_1 processes. $G(t)_{\text{Nb-Nb}}$ in the 5-at. % sample is also found to be a Gaussian, and $(T_2)_{\text{Nb-Nb}}$ changes from about 900 to about 700 μs with decreasing temperature.

Since we observe that the T_2 decay curves are exponentials in the spin-glass samples and that they decay much faster than $G(t)_{\text{Nb-Nb}}$ found in the non-spin-glass samples, we assume that $G(t)_{\text{Nb-Nb}}$ is not important in the T_2 decay of the spin-glass samples. Equation (8) becomes

$$M(t)/M_0 = \exp[-17.5t(T_{1P})_{\text{CE}}] \times \exp[-t/(T_2)_{\text{Fe}}]. \quad (11)$$

This is equivalent to

$$(1/T_2)_{\text{obs}} = 17.5/(T_{1P})_{\text{CE}} + (1/T_2)_{\text{Fe}}. \quad (12)$$

We find that $(T_2)_{\text{Fe}}$ has a linear temperature dependence above T_g in all three spin-glass samples.

$(T_{1P})_{\text{Fe}}$ of the 5- and 10-at. % samples is obtained by using Eq. (7). The maximum has been removed and $(T_{1P})_{\text{Fe}}$ decreases linearly with decreasing temperature below 77 K in the 5-at. % sample and above T_g in the 10-at. % sample (Fig. 5). Values of $(T_{1P})_{\text{Fe}}$ at 77 K are sensitive to the magnitude of $(T_{1P})_{\text{CE}}T$. In Fig. 5, $(T_{1P})_{\text{CE}}T=900$ ms is used, which causes the larger deviation at temperatures around 77 K. It is likely that this value would be modified at high-concentration samples. The observed regularity of the temperature dependence of $(T_{1P})_{\text{Fe}}$ and $(T_2)_{\text{Fe}}$ is another essential support of the justification of our postulates on the dominating relaxation mechanisms and the procedures to pull out the contribution of Fe spins from the raw data. From Eq. (9), this regularity also suggests a universal temperature dependence of τ , or the "spin-glass interaction," in different samples.

To see whether or not the correlation times and

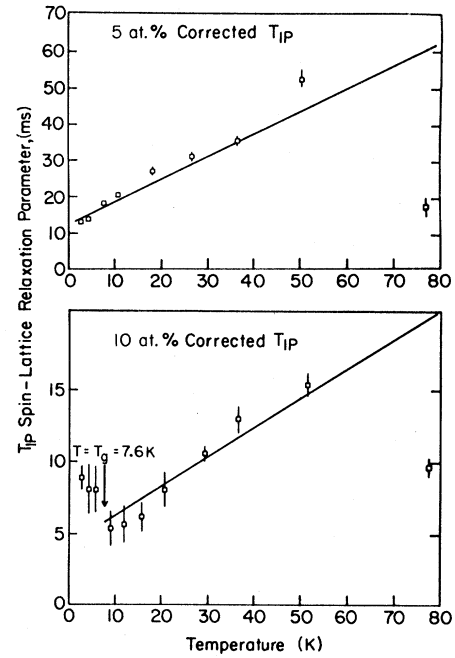


FIG. 5. $(T_{1P})_{\text{Fe}}$ of the 5- and 10-at. % samples obtained by removing $(T_{1P})_{\text{CE}}$ from the measured T_{1P} . $(T_{1P})_{\text{CE}}T=900$ ms is used.

the fluctuating local fields are isotropic in our spin-glass samples, we construct $(T_{1P}/T_2)_{\text{Fe}}$ from our $(T_{1P})_{\text{Fe}}$ and $(T_2)_{\text{Fe}}$ data. $(T_{1P}/T_2)_{\text{Fe}}$ at 77 K is, respectively, for the 8-, 10-, and 12-at. % samples, 16.0 ± 3.6 , 15.1 ± 3.6 , and 15.1 ± 3.6 , which are close to the predicted 17.5. It then jumps to about 28 ± 7 at lower temperatures, then makes another jump to about 42 ± 10 below T_g . We believe that this is probably a manifestation of the temperature dependence of the anisotropy in $2H\text{-NbSe}_2\text{Fe}_x$.

In a zero field and for temperatures above T_g , one does not expect the amplitude of the fluctuating field to change with temperature, as can be seen from the expressions for the fluctuating field in Eq. (2) and the coupling constant between Nb spins and Fe spins in Eq. (1). Then from Eqs. (5b) and (6b), the temperature dependence of $(T_{1P}/T_2)_{\text{Fe}}$ must indicate that μ_x , μ_y , and μ_z do not have the same correlation time and also that the amplitude of the fluctuating local field is anisotropic. In susceptibility measurements, a sharp cusp can only be detected when the measuring magnetic field is applied along the Z direction, which is perpendicular to the layer. Hall-coefficient measurements also show this anisotropy in the anomaly of the conduction-electron's scattering-off by Fe spins.¹⁵ We shall assign τ_x as the correlation time for μ_x and μ_y , and τ_z for μ_z . Then, we can write from Eqs. (5a) and (6a),

$$(T_{1P}/T_2)_{Fe} = 17 + k_{zz}/(k_{xx} + k_{yy}), \quad (13)$$

where k_{xx} , k_{yy} , and k_{zz} contain both contributions from τ_x and τ_z . The different temperature dependence of τ_x and τ_z causes $(T_{1P}/T_2)_{Fe}$ to deviate from 17.5 and vary with temperature. We shall discuss this point in more detail in Sec. VI C.

E. Intensity at 10.15 MHz

In the 5-at. % and more dilute samples, the intensity increases as the temperature is decreased (Fig. 6). In the spin-glass samples, the curves of intensity vs temperature all have a broad maximum and a very deep minimum (Fig. 6). The maxima occur at different temperatures for different samples. It is at 23, 37, and 43 K for the 8-, 10-, and 12-at. % samples, respectively. This can readily be explained by the interplay between Curie's law and the "spin-glass interaction" which causes intensity loss when the temperature is lowered near T_g . The minima are at T_g in the 8-at. % ($T_g = 4$ K) and 10-at. % ($T_g = 7.6$ K) samples. In the 12-at. % sample, the minimum is not at $T_g = 12$ K, rather somewhere between 16 and 20 K. We cannot pin down the position of this minimum more accurately because of the extremely small signal around the minimum. A good parameter to be plotted to show the significance of the intensity result is intensity times temperature. This is exactly the number of the observed nuclei by Curie's law. In Fig. 7, one can see that, for all three spin-glass samples, roughly a constant number of nuclei is observed on the high-temperature side. At the minima, one detects only about 1% of the total Nb nuclei.

As mentioned in Sec. II C, no temperature dependence of the static magnetic broadening is expected in our NQR study above T_g . We already know that this is supported by the linewidth measurements on

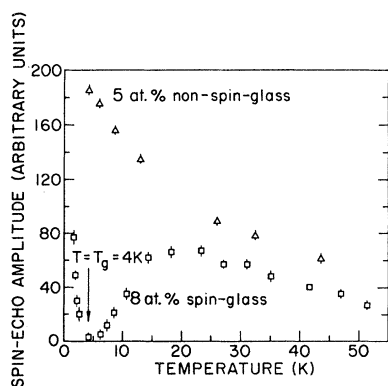


FIG. 6. Intensity as a function of temperature for the 5-at. % (non-spin-glass) and 8-at. % (spin-glass) samples. This figure shows the most striking difference between the non-spin-glass samples and the spin-glass samples.

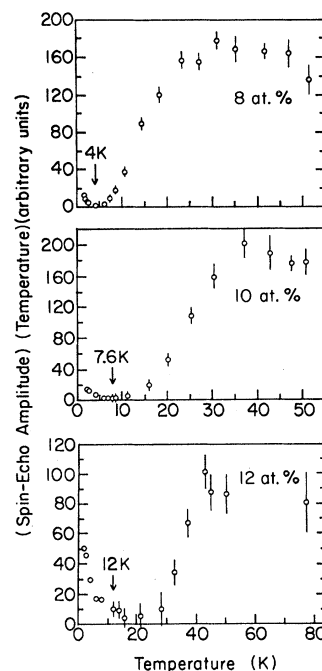


FIG. 7. Intensity-times-temperature as a function of temperature for three spin-glass samples. It can be clearly seen that for the 12-at. % sample, the minimum is definitely not at 12 K, the reported T_g by Hillenius and Coleman (Ref. 16).

the 10% samples: The linewidth at 23.1 K has the same value as that at 77 K. In the 10-at. % sample, 23.1 K is not a temperature close to T_g (7.6 K), but at this temperature only 40% of the Nb nuclei observed at higher temperatures is observed. Thus we can say that $H_1/\Delta H$ is constant above T_g in the spin-glass samples. The dramatic temperature dependence of the intensity in the spin-glass samples can then only be explained by the dynamic effect. There are different groups of Nb nuclei. Each one has a different value of T_2 , depending on its location relative to Fe spins, and each T_2 decreases with decreasing temperature as measured. As the temperature is lowered, only those groups of Nb nuclei with long enough T_2 at that temperature are still observable.

F. Susceptibility study

In order to solve the puzzle which arises from the discrepancy in the 12-at. % sample with regard to the temperature at which the sharp susceptibility cusp occurs (measured by Hillenius and Coleman) and the temperature where we find a deep intensity minimum, a T_{1P} and a T_2 minimum, we decided to set up a rig to measure the susceptibility of our

spin-glass samples. Qualitatively, we tested our rig, at first, by measuring the susceptibility of the 8-at. % sample. A sharp peak at about 4.6 ± 0.1 K is detected. This is consistent with Hillenius and Coleman's result. Then we did an empty coil test by going through the entire temperature range (25–2 K) twice, 24 hours apart. We found that the background signal not only is very flat over the entire temperature range but also has very good reproducibility.

In the 12-at. % sample, a sharp cusp is found at 19 ± 0.1 K which is more consistent with the intensity minimum (between 16 and 20 K) and the T_2 minimum than 12 K. Hillenius and Coleman used single crystals in their susceptibility measurements, while our 12-at. % sample is powder. Two samples possibly come from different batches, so they likely have different Fe concentrations. In $2H\text{-NbSe}_2\text{Fe}_x$, T_g is rather sensitive to the change of Fe concentration when the concentration is over 12-at. %. For example, 25 and 45 K have been reported as the T_g 's for the 15- and 18-at. % samples, respectively. In any event, what is important for our study is not the exact knowledge of the iron concentration, but rather the knowledge of the temperature of the susceptibility cusp to compare with our various NQR data.

VI. THE CORRELATION-TIME MODEL

For the sake of simplicity, Eq. (9) (the isotropic model) will be used to illustrate our model calculation. A more complicated model involving two correlation times (the anisotropic model) will be used to get the temperature dependence of τ_x (for μ_x and μ_y) and τ_z (for μ_z).

A. The isotropic model

The explanation of the drastic intensity loss due to the dynamic magnetic effects implies a distribution of T_2 . If one assumes an averaged correlation time τ for all Fe spins, it would also imply, by Eq. (9), a distribution of fluctuating local fields h_L , whose magnitudes depend on the distance between Nb nuclei and Fe spins. Then for a given τ at each temperature, there exists an h_m such that any Nb nucleus seeing a fluctuating local field larger than this h_m would have too short a T_2 to be observed. As τ changes with the temperature, h_m also changes. At the intensity minimum, only those Nb nuclei seeing very small h_L are observed.

An essential need of our model is a method to calculate h_m . We propose that this h_m can be obtained from the intensity data. A distribution of fluctuating local fields produced by Fe spins at Nb sites is denoted as $P(h)$, which is normalized. Then,

$P(h)\delta h$ is the probability of finding a Nb nucleus sitting in between h and $h + \delta h$. To get the number of Nb nuclei seeing a local field smaller than and equal to h_m , we simply integrate $P(h)$ from 0 to h_m . So, the intensity times temperature at each temperature can be used to get the value of h_m at that temperature.

Since our model claims a distribution of T_2 and h_L , we rewrite Eq. (9) as

$$\langle 1/(T_2)_{\text{Fe}} \rangle = \langle h_L^2 \tau \rangle = \langle h_L^2 \rangle \tau, \quad (14)$$

where the angular brackets mean an average over all the observed Nb nuclei. In writing Eq. (14), we assume that h_L^2 and τ can be averaged independently, although we have no proof that this is justified. The fact that we observed only a single $(T_2)_{\text{Fe}}$ over the entire measuring temperature range indicates that the observed $1/(T_2)_{\text{Fe}}$ is simply the averaged one on the left-hand side of Eq. (14). Some cross-relaxation mechanism must exist and be efficient enough to produce a unique $(T_2)_{\text{Fe}}$ among all the Nb nuclei. $\langle h_L^2(T) \rangle$ can be determined by

$$\langle h_L^2(T) \rangle = \left[\int_0^{h_m} h^2 P(h) dh \right] / \left[\int_0^{h_m} P(h) dh \right]. \quad (15)$$

The validity of Eq. (14) is based on two assumptions, besides the assumption of the isotropy of the correlation times: (1) $\omega_r \tau \ll 1$, where ω_r is the measuring rf frequency and (2) $\gamma h_L \tau \ll 1$, the motional narrowing limit. The motional narrowing limit is supported, at least above T_g , by the following two observations: (1) By Mössbauer experiments on our 12 and 18 at. % ($T_g = 45$ K) samples,³³ the Fe atom is found to be in Fe^{+2} state, which is also confirmed by magnetic susceptibility measurements on $\text{Fe}_{1/4}\text{NbSe}_2$.³⁴ Fe has an orbital angular momentum, so the spin-lattice relaxation of Fe spins is fast due to the spin-orbital interaction. (2) The strength of the spin-spin interaction between Fe spins is roughly $k_B T_g$. The mutual spin-flip time is then about 10^{-11} s. The spin flips of Fe spins can change the local fields at Nb sites because Fe spins are at different distances from each Nb site.

B. Forms of the distribution function

To calculate $\langle h_L^2 \rangle$, we need an analytical form of $P(h)$. Since there exists no calculation of $P(h)$ in the literature of spin-glasses, we look for some possible mathematical forms.

Assuming that the Fe-CE exchange interaction is approximately isotropic just as the Nb-CE hyperfine interaction and also that the Fe-CE interaction is roughly represented by a delta function of position,

then by the second-order perturbation theory, the expression for the Fe-CE-Nb interaction should be similar to that for the Fe-CE-Fe interaction. Then the static local field at the Nb site is proportional to that at the Fe site, as is the dynamic local field. It is not unreasonable to assume that the static and dynamic functions have similar forms. We see that one possible source of the mathematical form for $P(h)$ at Nb sites is the distribution functions for the static local fields at Fe spin sites.

Various forms of $Q(h_e)$ for the static exchange field produced by Fe spins at other Fe spin sites have been calculated by the mean random field (MRF) approximation³⁵ or by computer simulation³⁶ utilizing the randomness feature of spin-glasses. The coupling constant J_{ij} in the Hamiltonian of the "spin-glass interaction" is chosen to be either a Gaussian function of distance between Fe spins or random with equal probability for $J_{ij} = +a/(R_{ij})^3$ and $-a/(R_{ij})^3$. The spins can also be either Ising spins or Heisenberg spins. There are four different situations out of these combinations. We shall assign the name "Ising I" to the case with Ising spins and Gaussian J_{ij} and "Ising II" to the one with Ising spins and random J_{ij} , and so on. The following four forms have been used:

Ising I:

$$2 \exp(-h_e^2/\Delta h^2)/(\pi^{1/2}\Delta h).$$

Ising II:

$$2/[\pi\Delta h(1+h_e^2/\Delta h^2)].$$

Heisenberg I:

$$4h_e^2 \exp(-h_e^2/\Delta h^2)/(\pi^{1/2}\Delta h^3).$$

Heisenberg II:

$$4h_e^2/[\pi\Delta h^3(1+h_e^2/\Delta h^2)^2].$$

Note that the above $Q(h_e)$ forms are also valid in the 2D case, except that the numerical coefficients in the expression of Δh 's are different from that in the 3D case.³⁷

Δh is the physical quantity needed to be calculated out explicitly. Its expression has been given for $Q(h_e)$,^{35,36} but we shall use the same expression for $P(h)$ also. The appropriate coupling constant for the Fe-CE-Nb interaction is used:

$$\Delta h = (\frac{2}{3})\pi^2 cn A_0, \quad (16)$$

where c is the Fe concentration. n is the number of sites per unit cell for Fe spins and we assign 2 to it in $2H\text{-NbSe}_2$. A_0 is the strength of the interaction at Nb sites from Fe spins at a distance of one lattice constant, and it can be roughly estimated from Eq.

(1) in the 3D case, and the corresponding expression in the 2D case.³⁷ In the 3D case, Δh is found to be about 2.6 kG for the 10-at. % sample. We might not get the right absolute value of Δh from Eq. (16), but it will not effect the deduced temperature dependence of τ . The qualitative behavior of $\tau(T)$ is determined by the experimental intensity data and the particular $P(h)$ forms.

For temperatures below T_g , one has to consider the decrease of the amplitude of the fluctuating local fields due to the appearance of static Fe magnetic moments. As shown in Eq. (4), the mean-square amplitude of the fluctuating local fields decreases approximately as $(1-q)$. Therefore, we assign $\Delta h'^2 = \Delta h^2(1-q)$ as the width of the distribution function for temperatures below T_g .

C. The anisotropic model

Equation 6(a) can be rewritten in the same way as Eq. (14):

$$\langle (1/T_2)_{\text{Fe}} \rangle = \gamma^2/2[\langle k_{zz} \rangle + 17(\langle k_{xx} + k_{yy} \rangle)], \quad (17)$$

where k_{xx} , k_{yy} , and k_{zz} contain contributions both from τ_x and τ_z . Since no susceptibility cusp is found in the directions parallel to the layer, we expect $\tau_x(T)$ shows no anomaly at $T = T_g$. τ_x consists of two parts: one part from the interaction with conduction electrons and the other from the interaction with other Fe spins. The latter produces a rate which increases with increasing Fe concentration.

Since the 5-at. % sample is not a spin-glass and its NQR intensity roughly follows Curie's law (Fig. 6), we do not expect the mean-square amplitude of the fluctuating local fields would change with temperature. The temperature dependence of $(T_{1P})_{\text{Fe}}$ in the 5-at. % sample must therefore come from the correlation time. $(T_{1P})_{\text{Fe}}$ varies linearly with T which suggests that the correlation time varies with $1/(b+T)$ in the 5-at. % sample, where b is a constant (Fig. 5). Then by assuming that τ_x in the spin-glass samples has the same temperature dependence as that in the 5-at. % sample, we can write

$$\tau_x = A_k/(b+T), \quad (18)$$

where A_k is a constant. b can be obtained from the slope and the intercept at $T = 0$ K of the $(T_{1P})_{\text{Fe}}$ vs T curve in the 5-at. % sample, which is $b = 6.82$. Note that b is determined mainly by points at low temperatures which follow $1/(b+T)$ fairly well. Equation (18) produces a temperature-independent τ_x at low temperatures, but τ_x possibly still has a temperature dependence. So another possible form of temperature dependence to be considered is a

Korringa relation:

$$\tau_x = B_k / T, \quad (19)$$

where B_k is also a constant. We shall analyze our data using both Eqs. (18) and (19).

The temperature dependence of τ_z gives all the anomalies in T_{1P} , T_2 , and the intensity versus temperature curves. Questions then arise as to the magnitudes of k_{xx} , k_{yy} , and k_{zz} . By Eq. (4), we can write

$$k_{xx} = k_{yy} = 2a_0^2 \tau_x + b_0^2 \tau_z, \quad (20)$$

$$k_{zz} = 2c_0^2 \tau_x + d_0^2 \tau_z. \quad (21)$$

In writing Eqs. (20) and (21), we assumed that the coupling constant between k_{xx} and μ_x (or μ_y) is the same as that between k_{yy} and μ_x (or μ_y). Then $(T_{1P}/T_2)_{\text{Fe}}$ [from Eq. (13)] is given by

$$(T_{1P}/T_2)_{\text{Fe}} = \frac{17 + (2c_0^2 \tau_x + d_0^2 \tau_z)}{[2(2a_0^2 \tau_x + b_0^2 \tau_z)]}. \quad (22)$$

The coefficients in Eqs. (20) and (21) will be deduced from the measured $(T_{1P}/T_2)_{\text{Fe}}$ values based on the following three assumptions: (1) $\tau_x \sim \tau_z$ at high temperatures ($T/T_g \gg 1$), (2) $\tau_z \gg \tau_x$ near T_g , and (3) all coefficients are temperature independent above T_g . $(T_{1P}/T_2)_{\text{Fe}} \sim 30$ at $T = T_g$ has been used, and we get $a_0^2 \gg b_0^2$ and $d_0^2 \gg c_0^2$. So the first term of Eq. (21) can be omitted. The relative magnitudes of three coefficients are obtained: $b_0^2 = 2/25 a_0^2$, $d_0^2 = 52/25 a_0^2$. Thus, we finally get

$$\langle (1/T_2)_{\text{Fe}} \rangle = \gamma^2 \langle 36.4 a_0^2 \rangle (0.934 \tau_x + 0.066 \tau_z) \quad (23)$$

for $T > T_g$. From Eq. (23), we can follow the isotropic model to get $\tau_x(T)$ and $\tau_z(T)$. $\langle h_L^2 \rangle$ in Eq. (14) is equivalent to $\langle 36.4 a_0^2 \rangle$ in Eq. (23), which can be calculated by Eq. (15) for each temperature from the intensity data.

To get $\tau_z(T)$, τ_x must be determined first. A_k in Eq. (18) and B_k in Eq. (19) can be obtained by choosing a suitable temperature and the corresponding $(T_{1P}/T_2)_{\text{Fe}}$ value to get the relative value of τ_z and τ_x at this temperature. We find $A_k = 3.09 \times 10^{-10}$, 1.53×10^{-10} , and 3.71×10^{-11} s, and $B_k = 2.7 \times 10^{-10}$, 1.35×10^{-10} , and 3.25×10^{-11} s for the 8-, 10-, and 12-at. % samples, respectively.

For temperatures below T_g , we have to take into account the spin-freezing phenomena. Since a susceptibility cusp is found only in the direction perpendicular to the layer (Z direction), we assume only μ_z develops a static moment below T_g . Then Eqs. (20) and (21) can be written as

$$k_{xx} = k_{yy} = 2a_0^2 \tau_x + b_0^2 \tau_z T / T_g, \quad (24)$$

$$k_{zz} = d_0^2 \tau_z T / T_g, \quad (25)$$

where T/T_g is used as an approximation for $(1-q)$. The width of the distribution of the fluctuating local fields will be adjusted accordingly as

$$\Delta h'^2 = \Delta h'^2 (34 + 2.4 T/T_g) / 36.4. \quad (26)$$

D. The results

We have tried all four forms of the field distribution function with two different forms of temperature dependence for τ_x given in Eqs. (18) and (19). The main common result is that $\tau_z(T)$ increases rapidly near T_g . For the particular case of Heisenberg-I $P(h)$, τ_z changes typically from 10^{-11} s to about 10^{-9} s (10^{-8} s in the 8-at. % sample) as T_g is approached from above. This is quite a large change as compared with the change of only a factor of 5 or 6 in $T_2(T)_{\text{Fe}}$.

In phase-transition theories of spin-glasses, $1/\tau(T)$ has been postulated to have the form

$$1/\tau(T) = a(T - T_g)^\beta. \quad (27)$$

It has the similar expression below T_g , but β could be different. The $\tau(T)$ given in Eq. (27) is the correlation time for the autocorrelation function $\overline{S(t)S(t+\tau)}$. Our $\tau_z(T)$, according to Eq. (4), is just the $\tau(T)$ in Eq. (27) in the Z direction after averaging over all Fe spins. Recent EPR experiments³⁸ on CuMn seem to indicate that the linewidth and the g shift become divergent at T_g . The deduced $1/\tau$ is found to follow Eq. (27) plus a constant term from the dipolar interactions between Fe spins, and the β is found to be around 1. In our case, the obtained $1/\tau_z(T)$ near T_g from Heisenberg-I $P(h)$ and Heisenberg-II $P(h)$ can be fitted fairly well in the same way for temperatures above T_g . But only Heisenberg-I $P(h)$ produces closer β values among three spin-glass samples (Fig. 8). Given τ_x in Eqs. (18) or (19), we have $\beta = 2.7 \pm 1.0$ or 2.5 ± 0.5 for the 8-at. % sample, 2.1 ± 0.5 or 2.8 ± 0.5 for the 10-at. % sample, and 2.8 ± 0.05 or 2.8 ± 1.0 for the 12-at. % sample. The most likely β is then 2.5 ± 0.5 for both cases.

Figure 9(a) shows $\tau_z \times T_g$ plotted as a function of T/T_g for the case that τ_x is given by Eq. (18), and Fig. 9(b) is obtained if Eq. (19) is used. Near T_g , almost all points from three spin-glass samples fall upon a single curve. This exhibits the scaling properties which spin-glasses are expected to possess. We see that the maxima of τ_z in the 10- and 12-at. % samples are quite broad. In Fig. 9(a), τ_z develops a shallow minimum at about $0.4T_g$ after passing a maximum at T_g . The overall change of τ_z below T_g is only about a factor of 3 for all three spin-glass samples. Because of the constant term in the denominator, Eq. (18) sets the shortest limit for

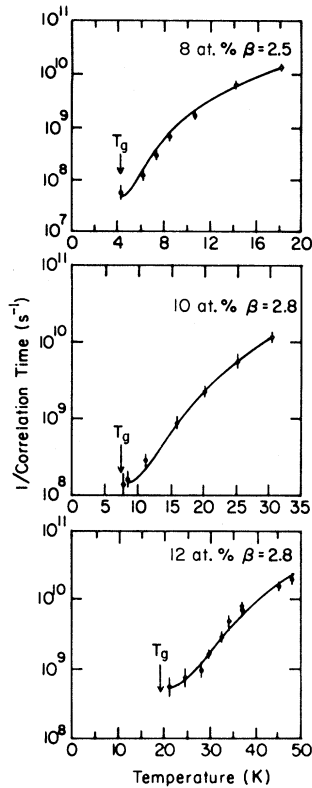


FIG. 8. $1/\tau_z$ vs temperature in three spin-glass samples. $\tau_x = B_k/T$ is used. The solid line is the result of the best fitting by Eq. (27) plus a constant term.

τ_x at low temperatures, which produces the longest τ_z from any possible temperature dependence of τ_x . Any temperature dependence of τ_x other than Eq. (18) only enhances the τ_z maximum, as is shown in Fig. 9(b).

We thus have obtained a temperature dependence of τ_z which is what a phase-transition theory of spin-glasses would predict: a maximum at T_g . After a critical slowing down at T_g , τ_z becomes shorter again with decreasing temperature below T_g . This kind of temperature dependence of τ_z not only gives a minimum in $T_{1P}(T)$ and $T_2(T)$ but also can easily explain the rapid intensity recovery below T_g . Experimentally, the number of the observed Nb nuclei recovers, relative to the high-temperature value, to 10% at $0.4T_g$ and up to 46% at $0.1T_g$. Because of the shorter correlation time, Nb nuclei with large h_L are becoming observable again at temperatures below T_g , despite the fact that there are also some Nb nuclei being wiped out of the range of our H_1 by the additional static broadening due to the spin freezing in the Z direction. The existence of the fast correlation time is supported by the recent neutron scattering experiments. In 1 at.% CuMn whose "spin-glass-interaction" strength is about the same

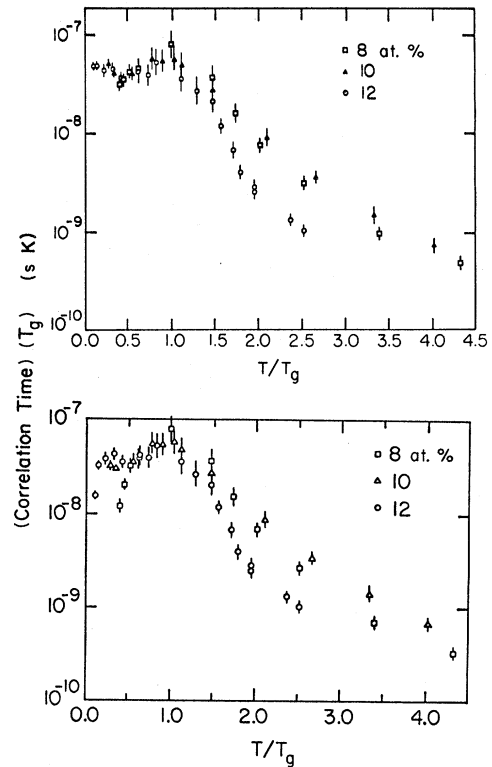


FIG. 9. (a) $\tau_z T_g$ plotted as a function for T/T_g for three spin-glass samples. This result is obtained by assigning $\tau_x = A_k/(T + 6.82)$. (b) The same plotting as in (a), but it is obtained by assigning $\tau_x = B_k/T$.

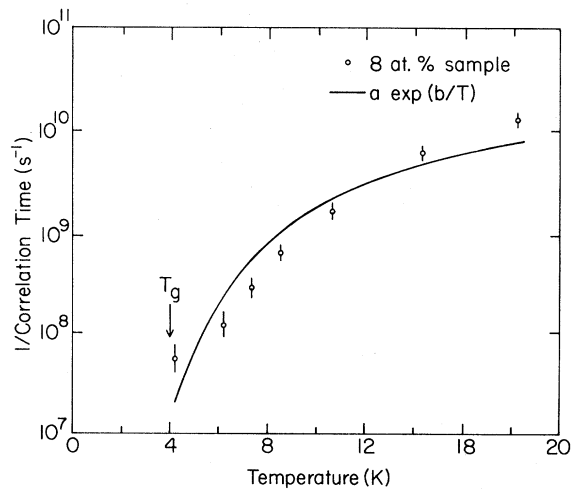


FIG. 10. $1/\tau_z$ vs temperature in the 8 at.% sample. The solid line is a best fitting by Arrhenius law. Compared with Fig. 8, it is clear that the deduced correlation times obey Eq. (27) plus a constant term better than Arrhenius law.

as our 10-at. % sample, the spectral density is found to peak at 10^{-11} s at $0.8T_g$.³⁹

There are still some unclear points in our model for temperatures below T_g . Owing to the spin freezing, the linewidth (ΔH) is expected to grow with decreasing temperature. So, $\Delta H/H_1$ is no longer a constant below T_g . Some corrections of the intensity-times-temperature values, which are unknown to us at present, must be made. The observable number of Nb nuclei influenced only by the fluctuating local fields should be higher than the measured value. Furthermore, the relative values of the coefficients before τ_z in Eqs. (24) and (25) may not simply be $(1-q)$ times those at temperatures above T_g . However, we do not expect that either of these uncertainties would change the essential result that τ_z has a maximum at $T=T_g$.

E. Problems with nonequilibrium models

If we assume that the correlation time is isotropic and use Eqs. (14) and (15), and $\Delta h'^2 = \Delta h^2(1-q)$ for temperatures below T_g , we get a correlation time which keeps increasing with decreasing temperature through T_g , although there is a significant change of slope at $T=T_g$. This behavior is close to what a nonequilibrium model predicts. But as we mentioned before, this isotropic model is not only inconsistent with the anisotropy in the susceptibility but also predicts a temperature-independent T_{1P}/T_2 ratio which contradicts our NQR results.

New μ SR (muon spin relaxation, time scale = 10^{-6} sec) techniques have been developed to allow the possible study of the μ^+ spin dynamics in spin glasses in a zero field or a longitudinal field. The correlation time in 1 at. % CuMn is observed to increase rapidly near T_g ,⁴⁰ and it keeps increasing smoothly with decreasing temperature through T_g .

In nonequilibrium models, τ possibly follows an Arrhenius law,⁵ $\tau = \tau_0 \exp(E/k_B T)$, or a Fulcher's law,¹⁴ $\tau = \tau_0 \exp\{E/[k_B(T-T_0)]\}$, where T_0 is a constant. When τ is long enough, i.e., $\gamma h_L \tau \sim 1$, at T_g to produce spin-freezing phenomena, the motional narrowing limit breaks down. Then we have $T_2 \sim \tau$ instead. As τ keeps increasing below T_g , T_2 increases again. Thus, we see that T_2 (or T_{1P}) minimum can qualitatively be explained by a nonequilibrium model.

But, some such models also predict that the number of loose spins (equivalent to the density of states of small-amplitude fluctuations) decreases exponentially with decreasing temperature below T_g .⁴² Experimentally, we observe a quite slow T_2 recovery and a rather fast intensity recovery. It is then clear that with the predicted temperature dependence of the number of loose spins, the fast intensity recovery

cannot be explained by the slow T_2 recovery below T_g .

In the particular case of our isotropic model calculation, it has been checked with computer fitting for all four field distribution functions that our deduced correlation time does not obey an Arrhenius law or a Fulcher's law (Fig. 10).

VII. CONCLUSION

From our NQR study, it is found that in those samples which are spin-glasses the relaxation processes of Nb nuclei are dominated by the interactions with Fe spins, which are describable by Redfield theory. The interactions with Fe spins cause anomalies in $T_{1P}(T)$, $T_2(T)$, and the intensity versus temperature curves at T_g . Based on the theory and the linewidth measurements as a function of temperature, it is concluded that the drastic intensity loss near T_g is due to a dynamic magnetic effect. More and more Nb nuclei must have too short a T_2 to be observed near T_g . The T_{1P}/T_2 ratio is found to deviate, at temperatures lower than 77 K, from a value of 17.5 predicted by Redfield theory for the isotropic fluctuating local fields. The deviation varies with temperature. This observation plus the anisotropy in the susceptibility lead us to conclude that $2H\text{-NbSe}_2\text{Fe}_x$ is an anisotropic spin-glass.

An anisotropic model is therefore constructed with the presumption that the correlation time for μ_x and μ_y shows no anomaly at T_g , since no susceptibility cusp is found on the X - Y plane. This model utilizes a distribution of fluctuating local fields to obtain, from the intensity data, the mean-square amplitude of the fluctuating fields seen by the observed group of Nb nuclei at each temperature. A maximum of the correlation time for μ_z 's, τ_z , is found at T_g for all three spin-glass samples. The magnitude of τ_z increases rapidly when T_g is approached from above. $1/\tau_z$'s functional form can be fitted with $b + a(T - T_g)^\beta$. Some closely similar values of β around a mean value of 2.5 are found for all three spin-glass samples. These results are best described by the phase-transition theories of spin-glasses.

ACKNOWLEDGMENTS

We are grateful to Professor R. V. Coleman for stimulating discussions, and for his kindness in supplying us with the samples with which we performed our experiments. We would also like to thank H. T. Stokes, B. H. Suits, C. D. Makowka, S. L. Rudaz, and J. K. Tsang for some helpful discussions. This research was supported in part by the Department of Energy, Division of Materials Sciences, under Contract No. DE-AC02-76ER01198.

- *Present address: Bell Telephone Laboratories, Murray Hill, NJ 07974.
- ¹V. Cannella, in *Amorphous Magnetism*, edited by H. O. Hooper and A. M. de Graaf (Plenum, New York, 1973), p. 195.
 - ²L. E. Wenger and P. H. Keesom, *Phys. Rev. B* **13**, 4053 (1970).
 - ³S. F. Edwards and P. W. Anderson, *J. Phys. F* **5**, 965 (1975).
 - ⁴J. L. Tholence and R. Tournier, *J. Phys. (Paris)* **35**, C4-229 (1974).
 - ⁵T. Moriya, *Prog. Theor. Phys.* **16**, 641 (1956); P. Heller, in *Proceedings of International School of Physics, Enrico Fermi*, edited by K. A. Müller and A. Rigamonti, (Societa Italiana D. Fisca, Bologna 1976), Vol. 59, p. 447.
 - ⁶S. Kirkpatrick and D. Sherrington, *Phys. Rev. B* **17**, 4384 (1978); T. Tanka, *Phys. Lett.* **75A**, 139 (1979); S. Kirkpatrick, in *Ordering in Strongly Fluctuating Condensed Matter Systems*, edited by T. Riste (Plenum, New York, 1980), p. 459.
 - ⁷D. A. Levitt and R. E. Walstedt, *Phys. Rev. Lett.* **38**, 178 (1977).
 - ⁸D. E. MacLaughlin and H. Alloul, *Phys. Rev. Lett.* **38**, 181 (1977).
 - ⁹K. Le Dang, P. Veillet, W. Nagele, and K. Knorr, *J. Phys. C* **13**, 6509 (1980).
 - ¹⁰H. Alloul, *Phys. Rev. Lett.* **42**, 603 (1979).
 - ¹¹A. K. Grover, L. C. Gupta, R. Vijayaraghavan, M. Matsumura, M. Nakano, and K. Asayama, *Solid State Commun.* **30**, 457 (1979).
 - ¹²D. Bloyet, E. Varoquaux, C. Vibet, O. Avenel, and M. P. Berglund, *Phys. Rev. Lett.* **40**, 250 (1978).
 - ¹³E. D. Dahlberg, M. Hardiman, R. Orbach, and J. Souletie, *Phys. Rev. Lett.* **42**, 401 (1979).
 - ¹⁴D. A. Whitney, R. M. Fleming, and R. V. Coleman, *Phys. Rev. B* **15**, 3405 (1977).
 - ¹⁵S. J. Hillenius, R. V. Coleman, E. R. Domb, and D. J. Sellmyer, *Phys. Rev. B* **19**, 4711 (1979).
 - ¹⁶S. J. Hillenius and R. V. Coleman, *Phys. Rev. B* **20**, 4569 (1979).
 - ¹⁷P. D. Antoniou, *Phys. Rev. B* **20**, 231 (1979).
 - ¹⁸C. Berthier, D. Jerome, and P. Molinie, *J. Phys. (Paris)* **C11**, 797 (1978).
 - ¹⁹S. Wada, *J. Phys. Soc. Jn.* **40**, 1263 (1976).
 - ²⁰D. E. MacLaughlin and M. Daugherty, *Phys. Rev. B* **6**, 2502 (1972); D. E. MacLaughlin and M. Daugherty, in *Amorphous Magnetism*, edited by H. O. Hooper and A. M. de Graaf (Plenum, New York, 1973), p. 245.
 - ²¹M. R. McHenry, B. G. Silbernagel, and J. H. Wernick, *Phys. Rev. B* **5**, 2958 (1972).
 - ²²C. Berthier, D. Jerome, P. Molinie, and J. Rouxel, *Solid State Commun.* **19**, 131 (1976).
 - ²³K. Yosida, *Phys. Rev.* **106**, 893 (1957).
 - ²⁴C. P. Slichter, *Principle of Magnetic Resonance*, 2nd ed. (Springer, Berlin, 1978), 2nd printing.
 - ²⁵D. E. MacLaughlin, J. D. Williamson, and J. Butterworth, *Phys. Rev. B* **4**, 60 (1971).
 - ²⁶B. E. Brown and D. J. Beerntsen, *Acta Crystallogr.* **18**, 31 (1965).
 - ²⁷D. M. Follstaedt and D. C. Barham (unpublished).
 - ²⁸W. R. Abel, A. C. Anderson, and J. C. Wheatley, *Rev. Sci. Instrum.* **35**, 444 (1964).
 - ²⁹C. M. Brodbeck, R. R. Burkey, and J. J. Hoeksema, *Rev. Sci. Instrum.* **49**, 1279 (1978).
 - ³⁰J. F. Garvin, Jr. and R. C. Morris, *Phys. Rev. B* **21**, 2905 (1980).
 - ³¹R. C. Morris, *Phys. Rev. Lett.* **34**, 1164 (1975).
 - ³²S. Wada, S. Nakamura, R. Aoki, and P. Molinie, *J. Phys. Soc. Jpn.* **48**, 786 (1980).
 - ³³Walter Weiss and Peter G. Debrunner (private communication).
 - ³⁴S. S. P. Parkin and R. H. Friend, *Philos. Mag.* **B41**, 65 (1980).
 - ³⁵M. W. Klein, *Phys. Rev.* **173**, 552 (1968); C. Held and M. W. Klein, *Phys. Rev. Lett.* **35**, 1783 (1975).
 - ³⁵L. R. Walker and R. E. Walstedt, *Phys. Rev. Lett.* **38**, 514 (1977).
 - ³⁷B. Fischer and M. W. Klein, *Phys. Lett.* **48A**, 329 (1974).
 - ³⁸M. B. Salamon, *Solid State Commun.* **31**, 781 (1979); M. B. Salamon, *J. Magn. Magn. Mater.* **15-18**, 147 (1980).
 - ³⁹A. P. Murani, F. Mezei, and J. L. Tholence, *Physica (Utrecht)* **B108**, 1283 (1981).
 - ⁴⁰Y. J. Uemura, T. Yamazaki, R. S. Hayano, R. Nakai, and C. Y. Huang, *Phys. Rev. Lett.* **45**, 583 (1980); Y. J. Uemura, K. Nishiyama, T. Yamazaki, and R. Nakai, *Solid State Commun.* **39**, 461 (1981).
 - ⁴¹G. I. Fulcher, *J. Am. Ceram. Soc.* **8**, 339 (1925); **8**, 789 (1925).
 - ⁴²D. A. Smith, *J. Phys. F* **4**, L266 (1974); F. A. de Rozario and D. A. Smith, *J. Phys. F* **7**, 439 (1977).